Published in final edited form as:

JACC Cardiovasc Imaging. 2019 July ; 12(7 Pt 1): 1165–1173. doi:10.1016/j.jcmg.2018.06.016.

Relative apical sparing of myocardial longitudinal strain is explained by regional differences in total amyloid mass rather than the proportion of amyloid deposits

Paco E. Bravo, MD[1,5], **Kana Fujikura, MD, PhD**[1], **Marie Foley Kijewski, PhD**[2], **Michael Jerosch-Herold, PhD**[1], **Sophia Jacob, BS**[2], **Mohamed Samir El-Sady, BS**[2], **William Sticka, CNMT**[2], **Shipra Dubey, PhD**[2], **Anthony Belanger, PhD**[2], **Mi-Ae Park, PhD**[2], **Marcelo F. Di Carli, MD**[1,2,3], **Raymond Y. Kwong, MD, MPH**[1,3], **Rodney H. Falk, MD**[3,4], and **Sharmila Dorbala, MD, MPH**[1,2,3,4]

[1]Noninvasive Cardiovascular Imaging Program; Brigham and Women's Hospital, Harvard Medical School, Boston, MA

[2]Division of Nuclear Medicine, Department of Radiology; Brigham and Women's Hospital, Harvard Medical School, Boston, MA, Noninvasive Cardiovascular Imaging Program

[3]Cardiovascular Division; Brigham and Women's Hospital, Harvard Medical School, Boston, MA, Noninvasive Cardiovascular Imaging Program

[4]Amyloidosis Program, Department of Medicine; Brigham and Women's Hospital, Harvard Medical School, Boston, MA, Noninvasive Cardiovascular Imaging Program,

[5]Divisions of Nuclear Medicine and Cardiology, Departments of Radiology and Medicine; Hospital of the University of Pennsylvania, Philadelphia, PA

Abstract

Objectives: To test whether relative apical sparing (RELAPS) of left ventricular (LV) longitudinal strain (LS) in cardiac amyloidosis (CA) is explained by regional differences in markers of amyloid burden [^{18}F-florbetapir uptake by PET and/or extracellular volume fraction (ECV) by cardiac magnetic resonance (CMR)].

Background: Further knowledge of the pathophysiological basis for RELAPS can help understand the adverse outcomes associated with apical LS impairment.

Methods: Prospective study of 32 subjects (62 ± 7 years, 50% males) with light chain CA. All subjects underwent 2D-echocardiography for LS estimation and ^{18}F-florbetapir PET for quantification of LV florbetapir retention index (RI). A subset also underwent CMR (n=22) for ECV quantification. Extracellular LV mass (LV mass*ECV), and total florbetapir binding

Correspondence to: Sharmila Dorbala, MD, MPH, Cardiac Amyloidosis Program, Cardiovascular Division, Department of Medicine, Heart & Vascular Center, Division of Nuclear Medicine, Department of Radiology, Brigham and Women's Hospital and Harvard Medical School, 70 Francis Street, Shapiro 5th Floor, Room 128, Boston, MA 02115. Tel: 617-732-6290; Fax: 617-582-6056; sdorbala@bwh.harvard.edu.

(extracellular LV mass*florbetapir RI) were also calculated. All parameters were measured globally, and regionally (base, mid and apex).

Results: There was a significant base-to-apex gradient in LS (−7.4±3.2 vs. −8.6±4.0 vs. −20.8±6.6%; P-trend<0.0001), maximal LV wall thickness (15.7±1.9 vs. 15.4±2.9 vs.10.1±2.4cm; P-trend<0.0001), and LV mass (74.8 ± 21.2 vs. 60.8 ± 17.3 vs. 23.4 ± 6.2g; P- trend<0.0001). In contrast, florbetapir RI (0.089 ± 0.03 vs. 0.097 ± 0.03 vs. 0.085 ± 0.03 μmol/min/g; P-trend=0.45), and ECV (0.53±0.08 vs. 0.49±0.08 vs. 0.49±0.07; P-trend=0.15) showed no significant base-to-apex gradient in the tissue concentration or proportion of amyloid infiltration, whereas, markers of total amyloid load such as total florbetapir binding (3.4 ± 1.7 vs. 2.8 ± 1.5 vs. 0.93 ± 0.49 μmol/min; P-trend <0.0001) and extracellular LV mass (40.0 ± 15.6 vs. 30.2 ± 10.9 vs. 11.6 ± 3.9g; P-trend <0.0001) did show a marked base-to-apex gradient.

Conclusion: Segmental differences in the distribution of the total amyloid mass, rather than the proportion, of amyloid deposits appear to explain the marked regional differences in LS in CA. While these two matrices are clearly related concepts, they should not be used interchangeably.

Keywords

longitudinal strain; amyloidosis; florbetapir; ECV; wall thickening

INTRODUCTION

Left ventricular (LV) longitudinal strain (LS) by speckle-tracking echocardiography is an independent predictor of mortality in amyloidosis.(1) While global LS is universally impaired in subjects with clinically manifest cardiac amyloidosis, the apical segments of the LV are typically less affected or even spared in some cases, a finding consistently observed in both light chain (AL) and transthyretin (ATTR) amyloidosis.(1,2) Importantly, emerging data also suggest that apical LS is probably a better predictor of events than LS at the basal or mid LV segments.(2)

The basis for the relative apical sparing of LS (RELAPS) in amyloidosis remains incompletely understood. Prior data suggests that it may be related to lower amyloid burden at the LV apical segments. This is suggested by the preferential thickening of the basal and mid LV segments(3) relative to the apical LV segments, coupled with an increase in either late gadolinium enhancement (LGE) on cardiac magnetic resonance (CMR)(2) or regional uptake of technetium-99m pyrophosphate (PYP) on single photon emission computed tomography (SPECT)(4). However, both LGE-CMR and PYP-SPECT are limited techniques for regional quantitative analyses because: 1) they are not fully quantitative, 2) LGE may not be detectable in cases of early or diffuse myocardial infiltration(5), and 3) measurement of relative apical uptake on SPECT is subject to significant partial volume error; furthermore, PYP is insensitive to AL. In contrast, contrast-enhanced (CE)-CMR imaging with T1 mapping and molecular targeted imaging with ^{18}Fluorine florbetapir positron emission tomography (PET) are advanced noninvasive techniques that can, potentially, provide more accurate estimation of amyloid burden in the heart compared to echocardiography, standard LGE, or SPECT. Native post-contrast T1 mapping permits measurement of global and regional LV extracellular volume fraction (ECV), which is significantly expanded in amyloid

hearts as a result of amyloid infiltration.(6,7) Florbetapir is a stilbene derivative that specifically binds to AL and ATTR deposits in human hearts ex-vivo and in-vivo,(8,9) and molecular amyloid PET imaging provides a unique opportunity to specifically quantify global and regional amyloid burden in the heart. However, whether the RELAPS phenomenon is explained by regional differences in amyloid burden has not been investigated.

The aims of the present study were 1) to measure the regional distributions of myocardial ^{18}F-florbetapir uptake, and ECV expansion in subjects with AL cardiac amyloidosis, and 2) to determine whether regional differences of these non-invasive markers of amyloid burden could help explain the relative sparing of apical LS phenomenon in this population.

METHODS

Study design and subjects:

A total of 32 subjects with AL cardiac amyloidosis were prospectively recruited, including 10 patients who had previously participated in a pilot study,(10) and 22 patients who are part of an ongoing clinical trial. All 32 subjects underwent echocardiography and myocardial ^{18}F-florbetapir PET, and 22 patients were additionally investigated with CE-CMR. Immunoglobulin AL amyloidosis was diagnosed in all subjects using standard criteria.(11) Cardiac involvement was diagnosed by 1) positive endomyocardial biopsy with typing of amyloid by immunohistochemistry or mass spectroscopy (n=18, 43%), or 2) typical echocardiographic findings of amyloid heart disease (LV wall thickness >11 mm, bright echogenic myocardium, evidence of restrictive physiology), and elevated troponin T or age-adjusted NT pro BNP. Subjects with ATTR cardiac amyloidosis and patients with AL amyloidosis but without cardiac involvement were not included in this study. This study was approved by the Partners Human Research Committee. Each study subject provided written informed consent.

Echocardiography:

2D echocardiography was performed in all subjects using standard clinical protocol per ASE recommendations.(12) Conventional analysis of the left ventricle included measurements of wall thickness, LV ejection fraction (LVEF), and diastolic parameters. Deformation analysis of the left ventricle based on 2D speckle-tracking imaging was performed offline using dedicated software (Image Arena v. 4.6; TomTec, Germany).

^{18}F-florbetapir PET/CT:

Individuals were positioned with the help of a CT topogram and a low-dose CT scan of the heart was acquired for attenuation correction of PET emission data. ^{18}F-florbetapir (~ 222–370 MBq [6.0 −10.0 mCi]) was injected through an IV catheter 1 minute after the start of a 60-min list-mode 3-D PET cardiac acquisition. Myocardial retention of ^{18}F-florbetapir, defined as the activity concentration in myocardial tissue between 10 and 30 minutes, normalized to the integral of the image-derived arterial input function (Supplementary Figure 1), was determined using Carimas v. 2.9 (Turku PET Centre, Finland). Myocardial florbetapir retention units are per gram of tissue (μmol/min/g). Therefore, total florbetapir

binding was also calculated by multiplying florbetapir RI by the extracellular LV mass component (see below).

Contrast-enhanced CMR (n=22):

All CMR images were acquired on a 3.0-T system (Tim Trio, Siemens, Erlangen, Germany), with electrocardiographic gating and breath holding. The protocol consisted of steady-state free-precession cine imaging for assessing ventricular function and morphology, and native and post-contrast T1 mapping for quantification of myocardial ECV. Cine imaging was obtained from a standard stack of short-axis slices (8 mm thick, no gap) and 3 long-axis planes. Measurement of myocardial T1 was performed during a single breath-hold at end-diastole in 3 short-axis slice positions, at the basal, mid and apical LV levels, by using the modified Look-Locker inversion recovery (MOLLI) method (Supplementary Figure 2).(13) T1 mapping images were acquired in the same 3 LV short-axis slices, once before (native T1) and 2 times, at 10, and 20 minutes (post-contrast T1), after the injection of 0.1 mmol/kg of gadoterate meglumine (Dotarem, Guerbet LLC USA). ECV was calculated from the formula: (1-hematocrit) = $(1/T_{1\ \text{Myo Post}} - T1_{\ \text{Myo Pre}})/(1/T1_{\ \text{Blood Post}} - 1/T1_{\ \text{Blood Pre}})$. Global myocardial ECV for an individual was calculated by averaging the myocardial segmental ECV values from the short-axis slices at the base, mid, and apical LV level (Supplementary Figure 2 E-F). Subsequently, the extracellular and cellular LV mass components were calculated from the following formulas: 1) extracellular LV mass = LV mass*ECV, and 2) cellular LV mass = LV mass*(1-ECV).(7,14)

Commercially available software (MedisSuite 3.0 Medical Imaging Systems, Leiden, the Netherlands) was used to post-process and quantify LV volumes, ejection fraction, mass, wall thickness, dimensions, fractional shortening and wall stress *(WS = 1.35 × LVSP × A_c/A_w*, where 1.35 is a conversion factor from mmHg to 1000dyn/cm^2; LVSP = non-invasive systolic blood pressure; A_c = LVED cavity area; and A_w = LVED wall area).(15) Measurements were obtained globally (when applicable) and segmentally at the basal, mid and apical level (Supplementary Figures 3–6). LV wall thickness was measured following a modified AHA17-segment model.

Comparison with reference CMR values:

Global and segmental functional, morphological and T1-mapping parameters were compared to established reference values (when available) for CMR in adults (Supplementary Tables 1–2).(7) (14) (16) (17)

Statistical Analysis

We analyzed the data using STATA (version 13.1). Continuous variables are shown as either mean ± standard deviation for normally distributed data or median [interquartile range] for nonnormal data. P-trend was used for testing for a significant base-to-apex gradient. Repeated measures ANOVA was performed to compare mean values of LV walls (heterogeneity), combined with Bonferroni's test for post-hoc analysis and correction for multiple comparisons. Simple correlations were assessed using longitudinal regression analysis and Pearson's correlation coefficient. Except for myocardial strain (derived from echocardiography), and ^{18}F-florbetapir uptake, all regional (basal-mid-apical LV)

parameters for this analysis were derived from CE-CMR. Finally, quartile groups were created based on maximal LV wall thickness. All statistical tests were 2-tailed, and a P value <0.05 was considered statistically significant.

RESULTS

Baseline characteristics for all 32 subjects included in the study are illustrated in Table 1. Half of AL subjects were males and about half were treatment-naive at time of enrollment. Lambda was the predominant monoclonal light chain, N-terminal pro-BNP was almost invariably elevated, and renal function was generally preserved or mildly impaired in most subjects. Echocardiography revealed the typical features of amyloidosis including small LV cavity, thickened LV walls, preserved LVEF, enlarged atria, and moderate to severe LV diastolic dysfunction (Table 1).

Global (when applicable) and regional echocardiographic, PET and CE-CMR imaging characteristics are summarized in Table 2. Mean global LS (−12.3% ± 7.7; min −5.03, max −19.4), but not CS (−21.3% ± 6.9; min −6.7, max-34.8) were significantly impaired, despite relatively preserved LVEF (53% ± 10; min 35, max 70) in most subjects. Regionally, LS, CS (Figure 1A-B), relative LVEF and fractional shortening showed a significant base-to-apex gradient, with the apical segments showing less dysfunction compared to the mid (P<0.001) and basal LV segments (P<0.001). LV mass, wall thickness (Figure 1C-D), volumes, and wall stress also showed a clear base-to-apex gradient, with the apical segments demonstrating significantly lower LV mass, wall thickness, and volumes (thus higher wall stress), compared to the basal (P<0.001) and mid wall segments (P<0.001).

^{18}F-florbetapir retention (0.089 μmol/min/g ± 0.03; min 0.05, max 0.17), and ECV (0.51 ± 0.07; min 0.38, max 0.63) were globally abnormal in all patients. Yet, regionally myocardial florbetapir retention, native T1, and ECV showed no statistically significant base-to-apex gradient. In contrast, total florbetapir binding and extracellular LV mass did show a marked base-to-apex gradient as expected (Table 2, Figure 2). Moderately strong regional correlations were observed between LS and markers of total amyloid load, but only weak with florbetapir RI or ECV. (Figure 3).

Comparison with reference CMR cohort:

Globally, indexed LV mass was 65% (86 ± 18 vs. 52 ± 13 g/m^2; P<0.0001), ECV 96% (0.51±0.07 vs. 0.26 ± 0.05; P<0.0001), and extracellular LV mass 152% (44 ± 14 vs. 13.6 ± 1.7 g/m^2; P<0.0001) greater, whereas cellular LV mass (42 ± 8 vs. 44 ± 10 g/m^2; P=0.40) was comparable, compared to reference adults (Supplementary Table 1). Regionally, average LV wall thickening at the base (12.3 ± 1.5mm), mid (10.7 ± 2.0mm) and apex (7.6 ± 1.9mm) corresponded to a 65%, 67% and 21% increment of the reported average LV wall thickness at the basal (7.5 ± 1.3mm), mid (6.4 ± 1.2mm) and apical (6.3 ± 1.1mm) segments of normal individuals (Supplementary Table 2).

Regional mass contribution to global LV mass was 47% ± 5 for the basal-, 38% ± 4 for the mid-, and 15% ± 3 for the apical-LV segments (Table 2). This mass relation was maintained

across quartile groups of maximal LV wall thickness, and regional differences in LS were observed across all groups (Supplementary Figure 7).

DISCUSSION

We found that RELAPS in cardiac amyloidosis is most likely explained by regional differences in the distribution of total amyloid mass, and not the proportion of amyloid deposits as estimated by advanced PET and CE-CMR techniques.

One of our study aims was to first investigate the regional distribution of specific (florbetapir) and non-specific (ECV) probes of amyloid infiltration. Florbetapir is a stilbene derivative used in clinical practice as a potent marker of amyloid deposits in tissue.(18–21) In human hearts, florbetapir uptake co-localized remarkably well to histological extracellular AL amyloid deposits in autopsy derived myocardial tissue ex-vivo,(9) and also proved to be both sensitive and specific for detection of cardiac amyloidosis in-vivo.(8) CE-CMR, on the other hand, provides an estimate of the myocardial extracellular fractional distribution volume (ECV) derived from measurements of the myocardial tissue longitudinal relaxation time constant (T1) before and following the administration of an extra-cellular gadolinium-based contrast agent. In cardiac amyloidosis, ECV appears to reflect the amount of amyloid deposition in the extracellular space.(22) Prior studies have shown that ECV is universally expanded in cardiac amyloidosis, even in cases where focal LGE is absent (up to 24% in one series).(5)

Both imaging modalities yielded abnormal global results in all subjects, and yet we failed to observe a significant base-to-apex gradient. The most feasible explanation is that imaging results from these modalities reflect tissue concentration or proportion, rather than an estimate of the whole tissue mass of amyloid deposition. Specifically, myocardial florbetapir (RI) yields quantitative PET values per unit mass of tissue (concentration), while ECV is measured as the percent of tissue comprised of extracellular space (proportion). This is in contrast to LV wall thickening, a crude marker of total amyloid mass, which exhibited marked regional variation, wherein, LV wall thickening at the basal and mid-wall segments was at least 3-fold greater than at the apex, consistent with the fact that 85% of the total LV mass was concentrated between the basal and mid wall segments. Our study also confirmed prior observations that LV wall thickening in AL occurs almost exclusively from expansion of the extracellular matrix,(7) as the cellular myocardial mass remained preserved compared to published reference values,(7,14) and also showed that this extra-cellular LV mass is florbetapir-avid, thus, allowing for quantitative methods capable of estimating the total amyloid load in the heart.

Taken together, these data indicates that while the proportion of amyloid infiltration is not remarkably different across the LV myocardium, the total amyloid mass is disproportionately greater toward the basal and mid wall segments compared to the apex. These findings also illustrate the importance of differentiating total mass from the proportion of amyloid deposits in tissue, two related concepts that should not be used interchangeably, but also highlight the importance of integrating morphologic findings with tissue characterization to better estimate the total amyloid load in the myocardium.

Longitudinal strain is universally impaired in patients with symptomatic amyloid heart disease and, while not pathognomonic, RELAPS is consistently seen in all patients with this condition, and certainly supports its diagnosis. The leading hypothesis to explain the RELAPS phenomenon has been lesser amyloid infiltration at the apical, relative to the basal and mid wall segments. Our study not only confirms prior observations, but provides new insights into the pathophysiology of RELAPS in cardiac amyloidosis by revealing that total amyloid mass, and not the proportion of amyloid infiltration, is what most likely leads to the marked regional differences in LS seen in cardiac amyloidosis.

LIMITATIONS

There are several limitations in our study that require discussion. First, not every patient underwent PET and CE-CMR; consequently, most of our analyses are limited to 69%(n=22) of the study population. A control group is lacking; however, comparison with a well-established reference cohort was performed in an attempt to overcome this limitation and, in all likelihood, repeating this study using our own controls would not have changed the results or the conclusions. We evaluated a relatively small sample size, which may have affected the statistical power, so it is possible that reported trends may become significant in a larger study sample. We did not include patients with ATTR; it remains to be investigated whether our findings are applicable to those patients as well. Last, while our study reveals a strong association between regional changes in myocardial strain and LV mass, it does not allow for a direct mechanistic explanation, nor does it provide any insight as to why the basal and mid LV wall segments are disproportionately thickened relative to the apex. This will remain a topic of future investigation.

CONCLUSION

In summary, we observed that differences in the segmental distribution of total amyloid mass, and not the tissue concentration or proportion of amyloid deposits as estimated by advanced PET and CE-CMR techniques, is what determines the marked base-to-apex gradient of longitudinal strain (RELAPS) in cardiac amyloidosis. Our findings call for further methods that that can integrate both morphologic and tissue characterization findings to better estimate the total amyloid load in the heart.

Supplementary Material

Refer to Web version on PubMed Central for supplementary material.

Acknowledgments

FUNDING SUPPORT

PB and KF were supported by the NIH T32 training grant (1T32HL094301). SD, RF, MFK, MFD, MJH, RYK are supported by NIH RO1 grant (RO1 HL 130563); SD is supported by American Heart Association Grant (AHA 16 CSA 2888 0004).

Abbreviations

LS	Longitudinal strain
RELAPS	Relative apical sparing of LS
ECV	Extracellular volume fraction
RI	Retention index
CE-CMR	Contrast-enhanced cardiac magnetic resonance

REFERENCES

1. Quarta CC, Solomon SD, Uraizee I et al. Left ventricular structure and function in transthyretin-related versus light-chain cardiac amyloidosis. Circulation 2014;129:1840–9. [PubMed: 24563469]
2. Ternacle J, Bodez D, Guellich A et al. Causes and Consequences of Longitudinal LV Dysfunction Assessed by 2D Strain Echocardiography in Cardiac Amyloidosis. JACC Cardiovascular imaging 2016;9:126–38. [PubMed: 26777222]
3. Phelan D, Collier P, Thavendiranathan P et al. Relative apical sparing of longitudinal strain using two-dimensional speckle-tracking echocardiography is both sensitive and specific for the diagnosis of cardiac amyloidosis. Heart 2012;98:1442–8. [PubMed: 22865865]
4. Sperry BW, Vranian MN, Tower-Rader A et al. Regional Variation in Technetium Pyrophosphate Uptake in Transthyretin Cardiac Amyloidosis and Impact on Mortality. JACC Cardiovascular imaging 2017.
5. Banypersad SM, Sado DM, Flett AS et al. Quantification of myocardial extracellular volume fraction in systemic AL amyloidosis: an equilibrium contrast cardiovascular magnetic resonance study. Circulation Cardiovascular imaging 2013;6:34–9. [PubMed: 23192846]
6. Fontana M, Pica S, Reant P et al. Prognostic Value of Late Gadolinium Enhancement Cardiovascular Magnetic Resonance in Cardiac Amyloidosis. Circulation 2015;132:1570–9. [PubMed: 26362631]
7. Fontana M, Banypersad SM, Treibel TA et al. Differential Myocyte Responses in Patients with Cardiac Transthyretin Amyloidosis and Light-Chain Amyloidosis: A Cardiac MR Imaging Study. Radiology 2015;277:388–97. [PubMed: 25997029]
8. Dorbala S, Vangala D, Semer J et al. Imaging cardiac amyloidosis: a pilot study using (1)(8)F-florbetapir positron emission tomography. European journal of nuclear medicine and molecular imaging 2014;41:1652–62. [PubMed: 24841414]
9. Park MA, Padera RF, Belanger A et al. 18F-Florbetapir Binds Specifically to Myocardial Light Chain and Transthyretin Amyloid Deposits: Autoradiography Study. Circulation Cardiovascular imaging 2015;8.
10. Dorbala S, Vangala D, Bruyere J Jr, et al. Coronary microvascular dysfunction is related to abnormalities in myocardial structure and function in cardiac amyloidosis. JACC Heart failure 2014;2:358–67. [PubMed: 25023822]
11. Gertz MA, Comenzo R, Falk RH et al. Definition of organ involvement and treatment response in immunoglobulin light chain amyloidosis (AL): a consensus opinion from the 10th International Symposium on Amyloid and Amyloidosis, Tours, France, 18–22 April 2004. Am J Hematol 2005;79:319–28. [PubMed: 16044444]
12. Lang RM, Badano LP, Mor-Avi V et al. Recommendations for cardiac chamber quantification by echocardiography in adults: an update from the American Society of Echocardiography and the European Association of Cardiovascular Imaging. Eur Heart J Cardiovasc Imaging 2015;16:233–70. [PubMed: 25712077]
13. Messroghli DR, Radjenovic A, Kozerke S, Higgins DM, Sivananthan MU, Ridgway JP. Modified Look-Locker inversion recovery (MOLLI) for high-resolution T1 mapping of the heart. Magn Reson Med 2004;52:141–6. [PubMed: 15236377]

14. McDiarmid AK, Swoboda PP, Erhayiem B et al. Athletic Cardiac Adaptation in Males Is a Consequence of Elevated Myocyte Mass. Circ Cardiovasc Imaging 2016;9:e003579. [PubMed: 27033835]
15. Fujita N, Duerinekx AJ, Higgins CB. Variation in left ventricular regional wall stress with cine magnetic resonance imaging: normal subjects versus dilated cardiomyopathy. Am Heart J 1993;125:1337–45. [PubMed: 8480586]
16. Dabir D, Child N, Kalra A et al. Reference values for healthy human myocardium using a T1 mapping methodology: results from the International T1 Multicenter cardiovascular magnetic resonance study. J Cardiovasc Magn Reson 2014;16:69. [PubMed: 25384607]
17. Kawel-Boehm N, Maceira A, Valsangiacomo-Buechel ER et al. Normal values for cardiovascular magnetic resonance in adults and children. Journal of cardiovascular magnetic resonance : official journal of the Society for Cardiovascular Magnetic Resonance 2015;17:29. [PubMed: 25928314]
18. Hobbs JR, Morgan AD. Fluorescence Microscopy with Thioflavine-T in the Diagnosis of Amyloid. J Pathol Bacteriol 1963;86:437–42. [PubMed: 14068952]
19. Klunk WE, Wang Y, Huang GF, Debnath ML, Holt DP, Mathis CA. Uncharged thioflavin-T derivatives bind to amyloid-beta protein with high affinity and readily enter the brain. Life Sci 2001;69:1471–84. [PubMed: 11554609]
20. Biancalana M, Koide S. Molecular mechanism of Thioflavin-T binding to amyloid fibrils. Biochim Biophys Acta 2010;1804:1405–12. [PubMed: 20399286]
21. Khurana R, Coleman C, Ionescu-Zanetti C et al. Mechanism of thioflavin T binding to amyloid fibrils. J Struct Biol 2005;151:229–38. [PubMed: 16125973]
22. Campbell-Washburn AE, Price AN, Ellmerich S et al. Monitoring systemic amyloidosis using MRI measurements of the extracellular volume fraction. Amyloid : the international journal of experimental and clinical investigation : the official journal of the International Society of Amyloidosis 2013;20:93–8.

Clinical Perspectives

Competency in Medical Knowledge

Studying the mechanisms of infiltration of light chain amyloidosis and their clinical consequences on the heart are of utmost importance. In the present study, using advanced multimodality imaging techniques aimed at quantifying total amyloid load in the heart, we found that the increment in left ventricular wall thickness occurs exclusively as a result of diffuse expansion of the extracellular matrix from amyloid infiltration. Interestingly, the density of amyloid deposits and the expansion of the extracellular volume are proportionately comparable from base-to-apex. Yet, only 15% of the total amyloid load is concentrated at the apical segments, likely explaining the relative apical sparing of longitudinal strain observed in cardiac amyloidosis.

Translational Outlook

Using targeted PET probes and advanced tissue characterization techniques, it is now feasible to non-invasively estimate the total amyloid mass in the heart.

This may become an important clinical endpoint in future studies assessing treatment response in patients with light chain amyloidosis.

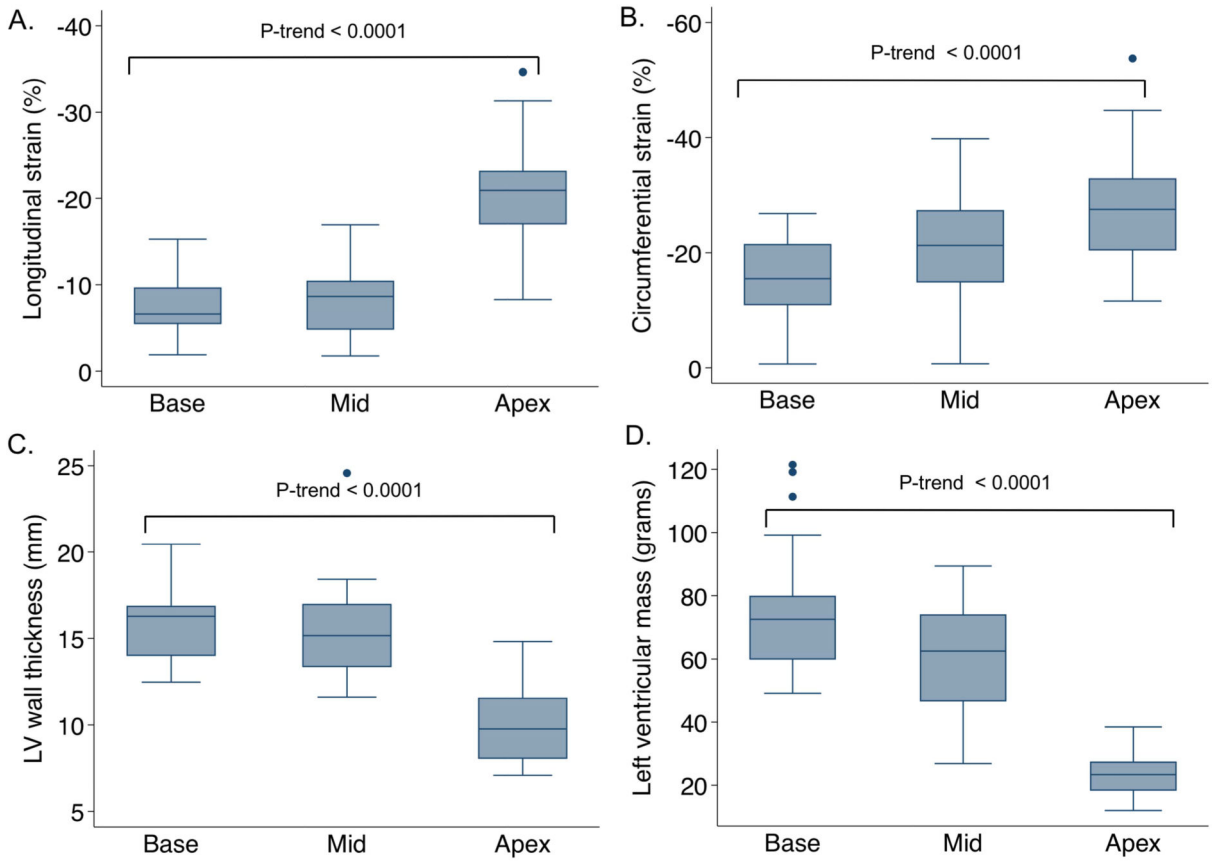

Figure 1. Base-to-apex gradient in myocardial strain, wall thickness and mass in cardiac amyloidosis

A significant base-to-apex gradient of left ventricular longitudinal strain (A), circumferential strain (B), wall thickness (C), and mass (D) is observed in cardiac light chain amyloidosis.

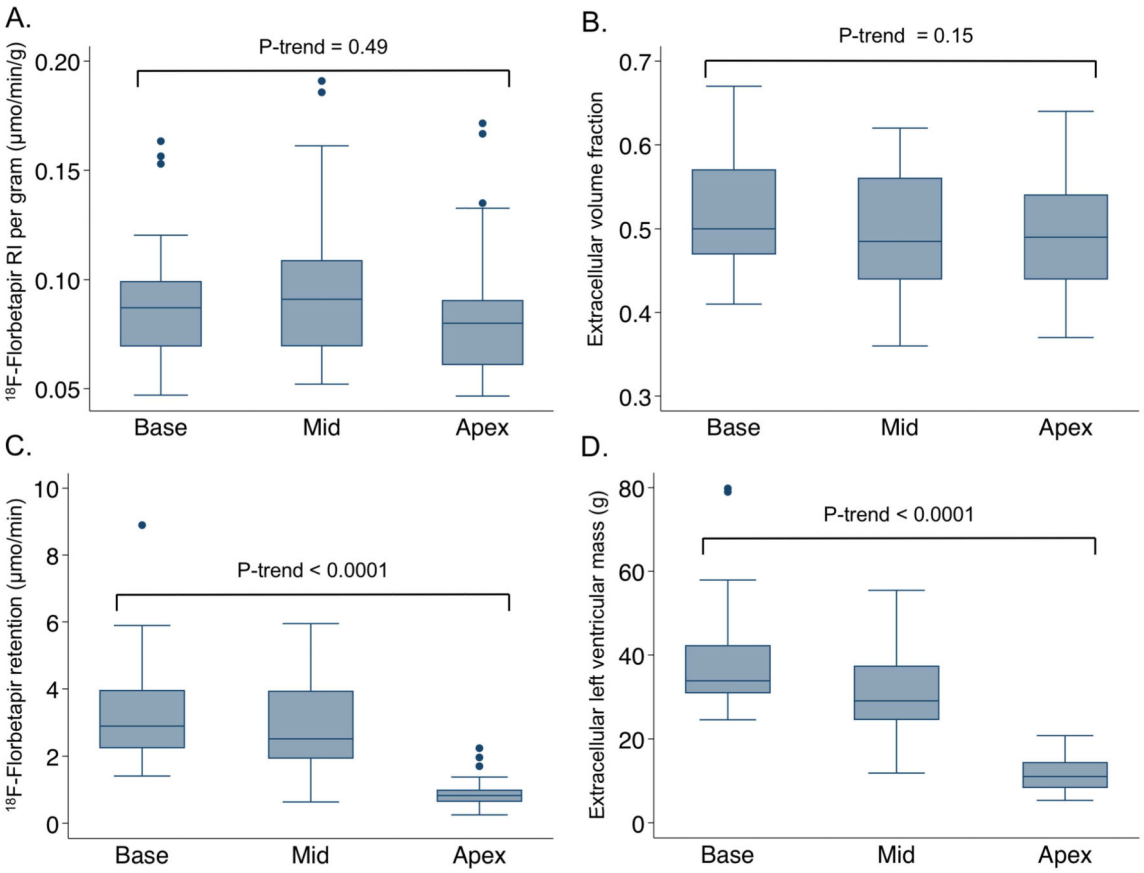

Figure 2. Differences in the distribution of markers examining tissue concentration versus total load of amyloid deposits

No significant base-to-apex gradient in the tissue concentration or proportion of amyloid infiltration according to ^{18}F-florbetapir retention (A) and extracellular volume fraction (B), respectively. In contrast, total ^{18}F-florbetapir binding (C) and extracellular LV mass (D), markers of total amyloid load, did show a marked base-to-apex gradient.

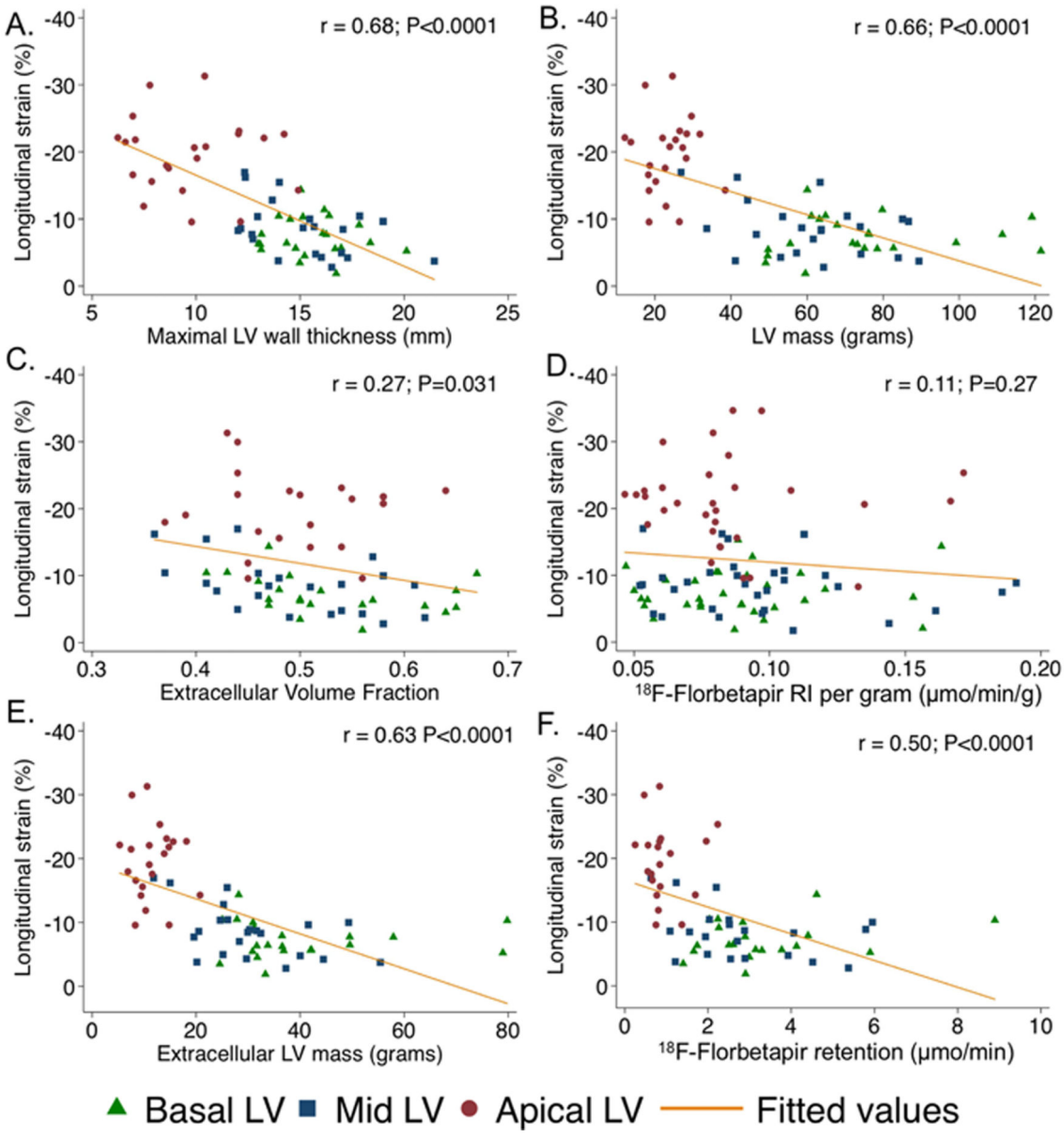

Figure 3. Regional correlations between myocardial strain and different markers of amyloid infiltration

Scatter graphs showing moderate to strong segmental correlations between longitudinal strain (y-axis) and markers of total amyloid load (A, B, E, F). In contrast, correlations between longitudinal strain with regional changes in the proportion (C) or tissue concentration (D) of amyloid deposits was weak

TABLE 1

Baseline Characteristics of Patients With Light Chain Amyloidosis (N = 32)

Age, yrs	62 ± 7
Male	16 (50)
History of prior chemotherapy	14 (44)
Laboratory	
Serum creatinine, mg/dl	1.15 ± 0.31
N-terminal pro-BNP, pg/ml	3631 (1,136–7,504)
Serum troponin, ng/ml	0.02 (0–0.1)
Serum free kappa, mg/dl	19.4 (12.2–37.3)
Serum free lambda, mg/dl	64.1 (14.2–172)
Kappa/lambda ratio, unitless	0.21 (0.10–1.27)
AL subtype: lambda AL	25 (78)
Echocardiography—chamber quantification	
Left ventricular end-diastolic volume index, ml/m^2	41 ± 13
Left ventricular end-systolic volume index, ml/m^2	19 ± 9
Left ventricular ejection fraction, %	55 ± 10
Basal septal wall thickness, mm	16.0 ±2.7
Basal inferolateral wall thickness, mm	16.3 ± 2.9
Left ventricular mass index, g/m^2	140 ± 39
Left atrial volume index, ml/m^2	35 ± 12
Echocardiography—Doppler parameters	
E/A velocity ratio, unitless	2.2 ± 1.0
Deceleration time, ms	170 ± 51
E/E′ lateral, unitless	19.9 ± 11.9
E/E′ medial, unitless	22.8 ±10.4
Tricuspid regurgitant peak velocity, m/s	2.50 ± 0.47

Values are mean ± SD, n (%), or median (interquartile range).

TABLE 2

Global (When Applicable) and Regional LV Differences of Imaging Characteristics Among Patients With Light Chain CA

	N	Global LV	Basal LV	Mid LV	Apical LV	p Trend*	p ANOVA†	p A vs. B	p A vs. M	p M vs. B
Echocardiography										
Longitudinal strain, %	32	−12.3 ± 7.7	−7.4 ± 3.2	−8.6 ± 4.0	−20.8 ± 6.6	<0.0001	<0.0001	<0.0001	<0.0001	0.76
Circumferential strain, %	32	−21.3 ± 9.5	−15.6 ± 6.9	−21.2 ± 8.3	−27.2 ± 9.5	<0.0001	<0.0001	<0.0001	< 0.001	<0.001
PET										
Florbetapir retention per gram, μmol/min/g	32	0.089 ± 0.03	0.089 ± 0.03	0.097 ± 0.03	0.085 ± 0.03	0.45	<0.0001	0.15	<0.0001	<0.0001
Cardiac MRI										
Native T1, ms	22	1212 ± 83	1189 ± 83	1207 ± 90	1233 ± 95	0.20	0.008	0.007	0.11	0.79
Extracellular volume fraction	22	0.51 ± 0.07	0.53 ± 0.08	0.49 ± 0.08	0.49 ± 0.07	0.15	0.0004	0.002	1.00	0.001
Maximal LV wall thickness, mm	22	15.9 ± 2.1	15.6 ± 1.8	15.1 ± 2.5	9.7 ± 2.6	<0.0001	<0.0001	<0.0001	<0.0001	0.81
LV mass, g	22	159 ± 40	74.8 ± 21.2	60.8 ± 17.3	23.4 ± 6.2	<0.0001	<0.0001	<0.0001	<0.0001	<0.0001
Regional/global LV mass, %	22		47 ± 5	38 ±4	15 ± 3	<0.0001	<0.0001	<0.0001	<0.0001	<0.0001
LVED volume, ml	22	130 ± 35	55.3 ± 16.6	55.5 ± 16.3	19.5 ± 6.0	<0.0001	<0.0001	<0.0001	<0.0001	1.00
LVES volume, ml	22	62 ± 26	30.5 ± 12.8	26.5 ± 13.0	5.0 ± 3.1	<0.0001	<0.0001	<0.0001	<0.0001	0.27
LVEF, %	22	53 ± 10	45.0 ± 14.0	53.6 ± 10.9	75.6 ± 10.9	<0.0001	<0.0001	<0.001	<0.001	0.015
Fractional shortening, %	22		21.4 ± 7.1	28.8 ± 8.9	43.1 ± 12.8	<0.0001	<0.0001	<0.0001	<0.0001	0.004
LV wall stress, 1,000 dyne/cm^2	22		112 ± 27	160 ± 55	254 ± 98	<0.0001	<0.0001	<0.0001	<0.0001	0.013
MRI and PET adjusted parameters										
Extracellular LV mass, g‡	22	81.1 ± 27.4	40.0 ± 15.6	30.2 ± 10.9	11.6 ± 3.9	<0.0001	<0.0001	<0.0001	<0.0001	<0.0001
Total florbetapir retention, μmol/min§	22	6.9 ± 3.5	3.4 ± 1.7	2.8 ± 1.5	0.93 ± 0.49	<0.0001	<0.0001	<0.0001	<0.0001	0.11

Values are n or mean ± SD.

*p value for trend (base-mid-apex or apex-mid-base).

†p value for repeated-measures ANOVA with Bonferroni correction to test for differences between apex (A) vs. base (B), apex (A) vs. mid LV (M), and mid LV (M) vs. base (B). All variables are shown as mean ± standard deviation.

‡Extracellular LV mass = LV mass*Extracellular volume fraction.

§Total florbetapir retention = Extracellular LV mass*Florbetapir retention per gram.

ANOVA = analysis of variance; CA = cardiac amyloidosis; LV = left ventricular; LVED = left ventricular end-diastolic volume; LVEF = left ventricular ejection fraction; LVES = left ventricular end-systolic volume; MRI = magnetic resonance imaging; PET = positron emission tomography.